ELSEVIER

International Journal of Mass Spectrometry 222 (2003) 63–73

International Journal of Mass Spectrometry

www.elsevier.com/locate/ijms

Application of ion mobility to the gas-phase conformational analysis of polyhedral oligomeric silsesquioxanes (POSS)

Jennifer Gidden, Paul R. Kemper, Erin Shammel, David P. Fee, Stanley Anderson[1], Michael T. Bowers*

Department of Chemistry and Biochemistry, University of California, Santa Barbara, CA 93106, USA

Received 3 April 2002; accepted 18 July 2002

Abstract

Ion mobility experiments and molecular modeling calculations were used to investigate the gas-phase conformational properties of various polyhedral oligomeric silsesquioxanes (POSS) cationized by sodium. POSS, $(RSiO_{3/2})_n$, has a rigid Si–O cage with organic substituents attached to each Si atom. Na^+POSS ions were formed by electrospray ionization (ESI) and matrix-assisted laser desorption/ionization (MALDI) and their collision cross-sections were measured in helium using ion mobility methods. Calculated cross-sections of theoretical models of the POSS ions, generated by molecular mechanics (MM) calculations, were compared to experiment for conformational identification. The calculations predict that the Na^+ ion remains outside of the Si–O cage and binds to one to two oxygen atoms in the cage or interacts with two neighboring organic substituents. Cross-sections of X-ray structures were also compared to the experimental and theoretical data to determine if any changes occur to POSS in the gas phase (compared to the condensed phase) and to provide a check for the geometries predicted by theory (which used untested Si parameters). Several types of POSS compounds were investigated that had different Si–O cage sizes (Si_6O_9, Si_8O_{12}, $Si_{10}O_{15}$, $Si_{12}O_{18}$, ...) and different "R" substituents such as cyclohexyl, cyclopropyl, vinyl, and phenyl groups. Experimental, theoretical, and X-ray cross-sections differed by <2% for each POSS compound. (Int J Mass Spectrom 222 (2003) 63–73)

Keywords: POSS; Ion mobility; Gas-phase conformational analysis

1. Introduction

Additives are commonly mixed with synthetic polymers in order to enhance or modify certain physical properties of the polymer. Typical additives include fillers, flame retardants, antioxidants, or plasticizers. These compounds are usually small, organic or inorganic molecules that are miscible with the polymer of interest or can be easily added to it during normal processing stages. However, a class of relatively large molecules containing organic and inorganic components called polyhedral oligomeric silsesquioxanes (POSS) [1,2] has recently been developed for incorporation into synthetic polymer systems. These nanocomposites are designed to help create hybrid polymeric materials that have higher thermal and chemical stability than traditional polymers, yet retain the polymer's processibility and commodity. Unlike

* Corresponding author. E-mail: bowers@chem.ucsb.edu
[1] Permanent address: Department of Chemistry, Westmont College, Santa Barbara, CA 93108, USA.

1387-3806/02/$ – see front matter
PII S1387-3806(02)00951-X

typical additives, POSS directly binds to the polymer chains.

POSS compounds have been around for some time, but only recently have they been sufficiently functionalized and developed for incorporation into traditional synthetic polymer systems. POSS has the chemical formula $(RSiO_{3/2})_n$ and consists of a highly symmetric, three-dimensional Si–O cage with various organic substituents (R) attached to each Si atom. A majority of the POSS molecules added to polymers have cubic Si–O cages, with 8 Si atoms forming the corners of the cube and 12 O atoms bridging each Si atom. They also generally contain seven inert functional groups (i.e., cyclohexane or cyclopropane) for solubility purposes and one reactive functional group (i.e., ester, epoxy, olefin, nitrile, etc.) for linking to the polymer chain. For example, POSS have been successfully linked to polyacrylates [3], polyurethanes [4], and polystyrenes [5] (among others), resulting in higher decomposition temperatures and oxidation resistance as well as reduced flammability and viscosity. POSS are generally synthesized with one or two reactive functional groups to avoid creating cross-linked networks, but some POSS molecules have been synthesized with multiple reactive functional groups for the expressed purpose of integration into polymer networks [6]. In monomeric or polymeric forms, POSS has numerous applications in materials, biological systems, and electronics.

Current interests in POSS have begun to focus on exploring the details of how its cage structure affects the polymer to which it is attached. While it is known that thermal and oxidative properties of synthetic polymers change when a certain amount of POSS is added, detailed structure–property relationships are still relatively unknown at this point. For example, it is not always known where the POSS molecule attaches to the polymer chain (near the middle or near the ends) or if multiple POSS are attached, how far they are from each other. It is also unclear how the conformation of the polymer chain changes when POSS is added or how the polymer actually interacts with the POSS cage. Another area of interest is understanding how the geometry and functionality of the POSS cages can be modified to induce specific physical changes in the polymer.

X-ray crystallography and NMR spectroscopy are usually used to obtain structural data on POSS molecules, but POSS–polymer systems can be difficult to examine with these methods. Synthetic polymers exist as a mixture of chain lengths and so data can only be obtained for the entire polymer distribution as a collective using these methods. Detailed information about how POSS interacts with one particular polymer chain is almost impossible to obtain. However, we have developed methods based on mass spectrometry and ion mobility [7,8] that may simplify the problem and answer some key questions about the structures and conformations of POSS–polymer systems. Ion mobility is based on the measurement of the amount of time it takes for an ion to drift through a buffer gas under the influence of a weak electric field. This drift time inherently contains information about the conformation of the ion. Different shaped ions have different collision cross-sections and hence different mobilities (and drift times) when drifting through the gas. Various computational methods are then used to generate model structures of the ions and calculate their cross-sections for comparison to experiment. By combining mass spectrometry with the ion mobility experiments, conformational data can be measured one POSS–oligomer system at a time and detailed information about how the POSS molecules interact with the polymer chains can be obtained.

Our ion mobility and molecular modeling calculations have been successful in determining accurate conformational properties of several synthetic polymers such as polyglycols [9–11], poly(methyl methacrylate) [12], poly(ethylene terephthalate) [13], and polystyrene [14]. However, they have not been applied to the analysis of POSS molecules before. Therefore, before studying the conformations of POSS–polymer systems, we decided to first examine the conformations of individual POSS molecules, with known structures, so that the proper procedures and parameterizations needed to accurately analyze and model the Si–O cages could be developed and tested.

In this paper we report our initial results on the application of ion mobility to the structural analysis of various POSS compounds cationized by Na^+. Several condensed (complete Si–O cage) and incompletely condensed (partial Si–O cage with multiple Si atoms capped with OH, also called silanols) POSS compounds of different cage sizes (Si_6O_9, Si_8O_{12}, $Si_{10}O_{15}$, $Si_{12}O_{18}$, ...) have been investigated. Incompletely condensed POSS molecules are commonly used to create specific condensed POSS systems by capping with the appropriate reactive functional group. Several of the POSS compounds that are presented here are functionalized with cyclohexyl groups, but data has also been obtained for POSS functionalized with cyclopropyl, vinyl, and phenyl groups. X-ray structures have been previously obtained for most of these POSS compounds as well [14]. Collision cross-sections of these X-ray structures are compared to those obtained from the ion mobility measurements and the theoretical modeling to check the validity of the calculations and to determine if any structural changes occur when POSS is introduced to the gas phase.

2. Experiment

2.1. Instrumental setup

The ion mobility experiments were carried out on two separate, home-built instruments. These instruments are described in detail elsewhere [16,17], but they have the general setup shown in Fig. 1. The POSS compounds that were investigated are listed in Table 1 with their chemical formula and abbreviated name (used throughout this paper). Simple pictures of the fully condensed and incompletely condensed POSS cages are shown in Figs. 2 and 3.

Table 1
List of condensed and incompletely condensed POSS compounds

Name	Chemical formula
Cy_6T_6	$(C_6H_{11})_6(Si_6O_9)$
Bz_8T_8	$(CH_2–C_6H_5)_8(Si_8O_{12})$
Ph_8T_8	$(C_6H_5)_8(Si_8O_{12})$
$Vi_{10}T_{10}$	$(CH{=}CH_2)_{10}(Si_{10}O_{15})$
$Vi_{12}T_{12}$	$(CH{=}CH_2)_{12}(Si_{12}O_{18})$
$H_{14}T_{14}$	$H_{14}(Si_{14}O_{21})$
$Cp_4D_4(OH)_4$	$(C_5H_9)_4(Si_4O_4)(OH)_4$
$Cy_6T_4D_2(OH)_2$	$(C_6H_{11})_6(Si_6O_8)(OH)_2$
$Cy_7T_4D_3(OH)_3$	$(C_6H_{11})_7(Si_7O_9)(OH)_3$

The first ion mobility instrument has an electrospray ionization (ESI) [18] source followed by an ion funnel and the drift cell [16]. Solutions were prepared by mixing 100 μL of POSS (~1 mg/mL in chloroform) with 900 μL of acetone, 20 μL of formic acid, and 20 μL of NaI (saturated solution in acetone) and injected into the source at a rate of 20–50 μL/h. The voltage applied to the spray needle was ~2 kV. Ions travel from the ESI source to the drift cell via an ion funnel. This funnel consists of three sets of lenses (total 67) that compress the ion stream leaving the source and essentially act as a high-transmission ion guide.

For the ion mobility experiments, the next to last lens in the ion funnel is pulsed so as to gate the ions into the drift cell. (The ions are usually injected into the drift cell at 60–90 eV.) The gate is opened for about 10 μs and pulsed at a rate of 1–10 kHz. The drift cell, itself, is a cylindrical Cu tube, 4.5 cm long, filled with

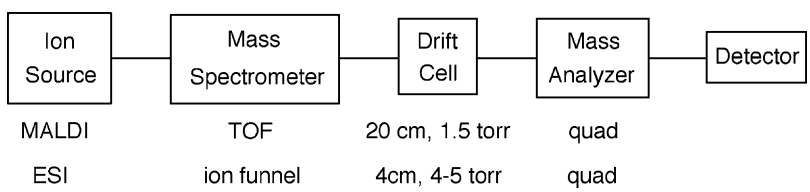

Fig. 1. Simple schematic of the instrumental setups used to measure mobilities (and collision cross-sections) of the Na^+POSS ions. One instrument contains an ESI ion source followed by an ion funnel (see text) and a 4.5 cm long, copper drift cell. The other instrument contains an MALDI ion source followed by a TOF mass spectrometer and a 20 cm long, glass drift cell.

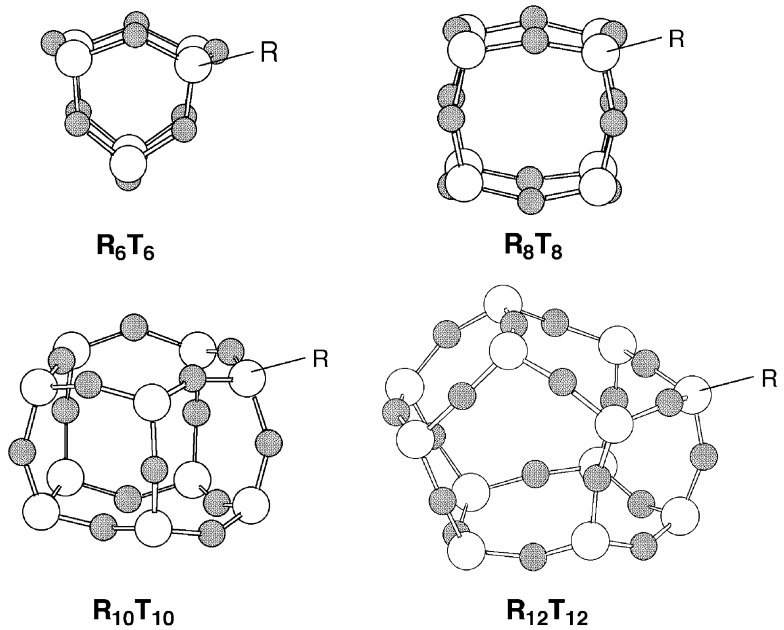

Fig. 2. Simple schematics of the condensed POSS compounds discussed in this paper. Silicon atoms are white and oxygen atoms are spotted. The "R" substituents include hydro, cyclohexyl, benzyl, phenyl, and vinyl groups.

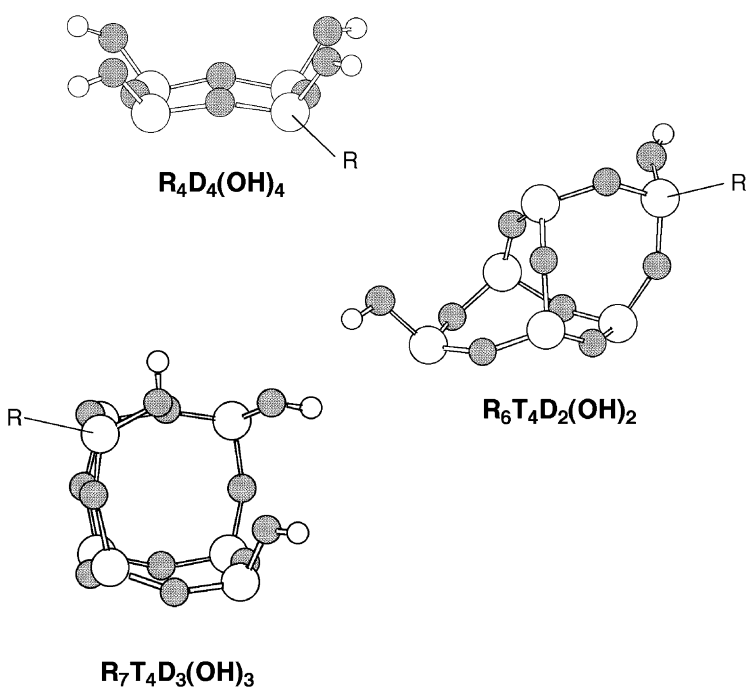

Fig. 3. Simple schematics of the incompletely condensed POSS compounds discussed in this paper. Silicon atoms are white and oxygen atoms are spotted. "R" substituents include cyclopentyl and cyclohexyl groups.

4–5 Torr of He. Four drift guard rings provide a uniform electric field across the cell that can be varied from 2–20 V/cm. Ions exiting the drift cell are mass selected with a quadrupole mass filter, thus allowing only the ion of interest to be detected, and collected as a function of time at the detector (the time is started with the pulsed gate), yielding an arrival time distribution (ATD). The quadrupole can also be scanned to obtain a mass spectrum of the ions formed in the source.

The second ion mobility instrument consists of a matrix-assisted laser desorption/ionization (MALDI) [19] source and a time-of-flight (TOF) mass spectrometer before the drift cell [17]. 2,5-Dihydroxybenzoic acid (DHB) was used as the matrix and tetrahydrofuran as the solvent. Approximately 100 μL of POSS (∼1 mg/mL) was mixed with 100 μL of DHB (100 mg/mL) and 15 μL of NaI (saturated solution in methanol), applied to a 2.8 cm long stainless steel cylinder, and dried. A nitrogen laser ($\lambda = 337$ nm) with a 10 ns pulse width operated at 50 Hz was used to generate the ions. One or two microseconds after the laser pulse, a 10 kV extraction voltage is applied to extract the ions from the source and send them through the TOF mass spectrometer. High-resolution mass spectra can be obtained by operating the TOF in the "reflectron" mode.

For the ion mobility experiments, the reflecting grids in the TOF are turned off to allow the ions to enter the drift cell. Two linear mass gates (with unit mass resolution at $m/z = 500$) are positioned before the drift cell to mass select the ions before they enter the mobility experiments, but they are not always activated. A quadrupole mass filter after the drift cell, with higher mass resolution, is usually used for allowing only the ion of interest to hit the detector. The ions are, however, always decelerated to 10–100 eV before injection into the drift cell. As opposed to the first ion mobility instrument described earlier, the drift cell in the MALDI-TOF instrument is a 20 cm cylindrical glass tube filled with ∼1.5 Torr of He. Twenty guard rings provide for the uniform electric field across the cell that can be varied between 5–15 V/cm. Ions exiting the cell are mass selected with a quadrupole mass filter and detected as a function of time, yielding an ATD. In this case, the timer is triggered with the application of the source extraction voltage.

2.2. Data analysis

The mobility of the ion, K_o, can be obtained from the arrival time distributions using Eq. (1) [20]

$$t_A = \left(l^2 \frac{273}{760T} \frac{p}{V} \frac{1}{K_o} \right) + t_o \quad (1)$$

where t_A is the ion's arrival time (taken from the center of the ATD peak), l is the length of the drift cell, T is temperature, p is the pressure of the He gas, V is the electric field strength, and t_o is the amount of time the ion spends outside of the drift cell. ATDs are typically measured for a series of different drift voltages and K_o is determined from a plot of t_A vs. p/V (the plot yields a straight line with a slope inversely proportional to K_o and an intercept of t_o).

Once K_o is known, the ion's collision cross-section, $\Omega^{(1,1)}$, can be obtained from kinetic theory [20]

$$\Omega^{(1,1)} = \frac{C_o}{K_o} \quad (2)$$

where C_o is a constant containing known parameters such as ion charge, He pressure, temperature, and the ion–He reduced mass. In short, the ion's arrival time is inversely proportional to its mobility and directly proportional to its collision cross-section. Compact ions with small collision cross-sections will drift through the cell faster (and have shorter arrival times) than more extended ions with larger collision cross-sections. Therefore, the ATDs inherently contain information about the overall shape or conformation of the ion.

2.3. Theoretical modeling

To obtain conformational details about the ions measured in the ion mobility experiments, cross-sections extracted from the ATDs are compared to calculated cross-sections of theoretical models. For large molecules (like POSS), molecular mechanics/dynamics (MM/MD) calculations are usually needed to generate the candidate structures. We have used the

AMBER [21] set of MM/MD programs to provide theoretical structures for a number of biological [22,23] and synthetic [10–14] polymers and observed very good agreement with experimental data. However, AMBER is not parameterized for Si-containing compounds like POSS. Therefore, as an approximation, Si parameters were taken from published ab initio calculations by Sun and Rigby [24] designed to provide CFF-type force field parameters for polysiloxanes, and incorporated into the AMBER database. Quantum mechanical calculations were also used to derive partial charges for the atoms using the RESP fitting model [25]. Since the Si parameters have not been tested, X-ray structures [15] for seven of the POSS compounds listed in Table 1 were used as a check for the geometries predicted by the theoretical models and for comparison to experimental data.

An annealing/energy minimization cycle is used to produce 50–100 low energy structures for each POSS compound. A given POSS structure is initially built using the X-ray data to obtain bond lengths and angles. The structure is then energy minimized, run through an MD simulation at 800 K for 30 ps, cooled to 0 K through an additional 10 ps MD simulation, and energy minimized again. The resulting structure is saved and used as the starting point for another annealing/minimization cycle. The entire process is repeated until 50–100 structures are obtained.

Once the structures are produced, their collision cross-sections must be calculated for comparison to experiment. A previously developed projection model [9,26,27], using appropriate atomic collision radii calculated from the ion–He interaction potential, was used to calculate the angle-averaged collision cross-section of each theoretical structure. A scatter plot of cross-section vs. energy is then used to help identify the ions observed in the ATDs. In most cases, the average cross-section of the lowest 3–5 kcal/mol structures is used for comparison to experiment. MD simulations at 300 K can also be performed for a given structure to determine thermally averaged cross-sections. These MD simulations are run for 1000 ps with cross-sections calculated every 1 ps. The average of the 1000 cross-sections is then compared to the experimental data. The "projection model" was also used to calculate the cross-sections of the POSS X-ray structures. In these cases, the calculations were repeated 10 times to get an average cross-section for the structure.

3. Results and discussion

Mass spectra of a mixture of $Vi_{10}T_{10}$ and $Vi_{12}T_{12}$ (with NaI added) are shown in Fig. 4. The top spectrum was obtained with the ESI instrument and the bottom spectrum with the MALDI-TOF instrument. Clean spectra, with little to no fragmentation, were obtained for all of the POSS compounds in both instruments (the cluster of peaks below $m/z = 300$ in the MALDI spectrum is due to the matrix). The two large peaks between $m/z = 800$–1000 are the sodiated $Vi_{10}T_{10}$ and $Vi_{12}T_{12}$ species ($Na^+Vi_{10}T_{10}$, $Na^+Vi_{12}T_{12}$) while the two smaller peaks at 22 lower mass units are the protonated species. When the laser was focused in the MALDI experiments, the protonated peaks disappeared from the mass spectrum (although no fragmentation was observed). The vinyl series and Cy_6T_6 (in the ESI experiments) were the only POSS compounds in which significant amounts of the protonated species were observed in the mass spectra.

Fig. 5 shows typical ATDs for the Na^+POSS ions measured at 300 K. These ATDs were obtained under similar experimental conditions (i.e., pressure, drift voltage, temperature). Single, symmetric peaks are observed for all of the Na^+POSS ions, indicating the ions either have single conformations or rapidly interconverting conformers [13,28]. The average arrival time increases with an increase in the size of the Si–O cage or with an increase in the size of the "R" substituent, consistent with an increase in cross-section. In order to obtain accurate mobilities (cross-sections), ATDs at several different drift voltages were measured. A typical plot of arrival time as a function of the drift voltage is given in Fig. 6 for $Na^+Vi_{10}T_{10}$ and $Na^+Vi_{12}T_{12}$. The slope of the line yields K_o and the intercept is t_o (see Eq. (1)). Collision cross-sections are determined from K_o using Eq. (2) and are listed in Table 2 for

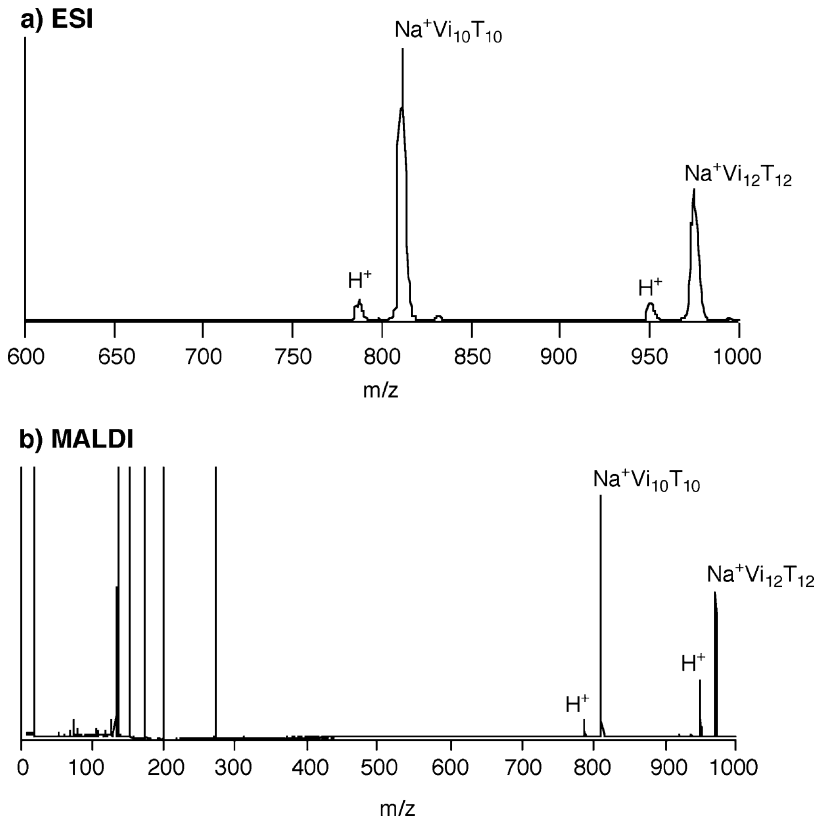

Fig. 4. ESI (a) and MALDI (b) mass spectra of a mixture of $Vi_{10}T_{10}$ and $Vi_{12}T_{12}$ (see Table 1) cationized by sodium. Clean spectra were obtained for all of the POSS compounds. The peaks below $m/z = 300$ in the MALDI spectrum are matrix peaks.

Table 2
Collision cross-sections (Å^2) of the POSS compounds

Name	X-ray[a]	ESI (Na^+)	MALDI (Na^+)	Theory (Na^+)
Cy_6T_6	224	221	225	222
Bz_8T_8	265			
Ph_8T_8		260	263	257
$Vi_{10}T_{10}$		189	193	192
$Vi_{12}T_{12}$	212	214	216	216
$H_{14}T_{14}$	137			139[b]
$Cp_4D_4(OH)_4$	154		157	153
$Cy_6T_4D_2(OH)_2$	222	220	222	222
$Cy_7T_4D_3(OH)_3$	248	247	254	251

[a] Structures obtained from Dr. Tim Haddad at ERC Inc., Air Force Research Laboratory.
[b] Calculated value for the neutral species.

all of the Na^+POSS compounds. Similar experimental cross-sections (~2% difference) are obtained for the Na^+POSS ions generated by ESI and those generated by MALDI. ATDs for the protonated species of Vi_nT_n and Cy_6T_6 yielded similar cross-sections as the sodiated species as well.

Also shown in Table 2 are the calculated cross-sections of POSS structures obtained from X-ray crystallography. Normally, X-ray data is not available for comparison to the ion mobility experiments and detailed conformational information about the ions is obtained from theoretical models. However, the goals of this study are to determine whether POSS retains its shape in the gas phase and to check the new Si parameters used in the theoretical modeling. Therefore, “known” structures were needed to serve as

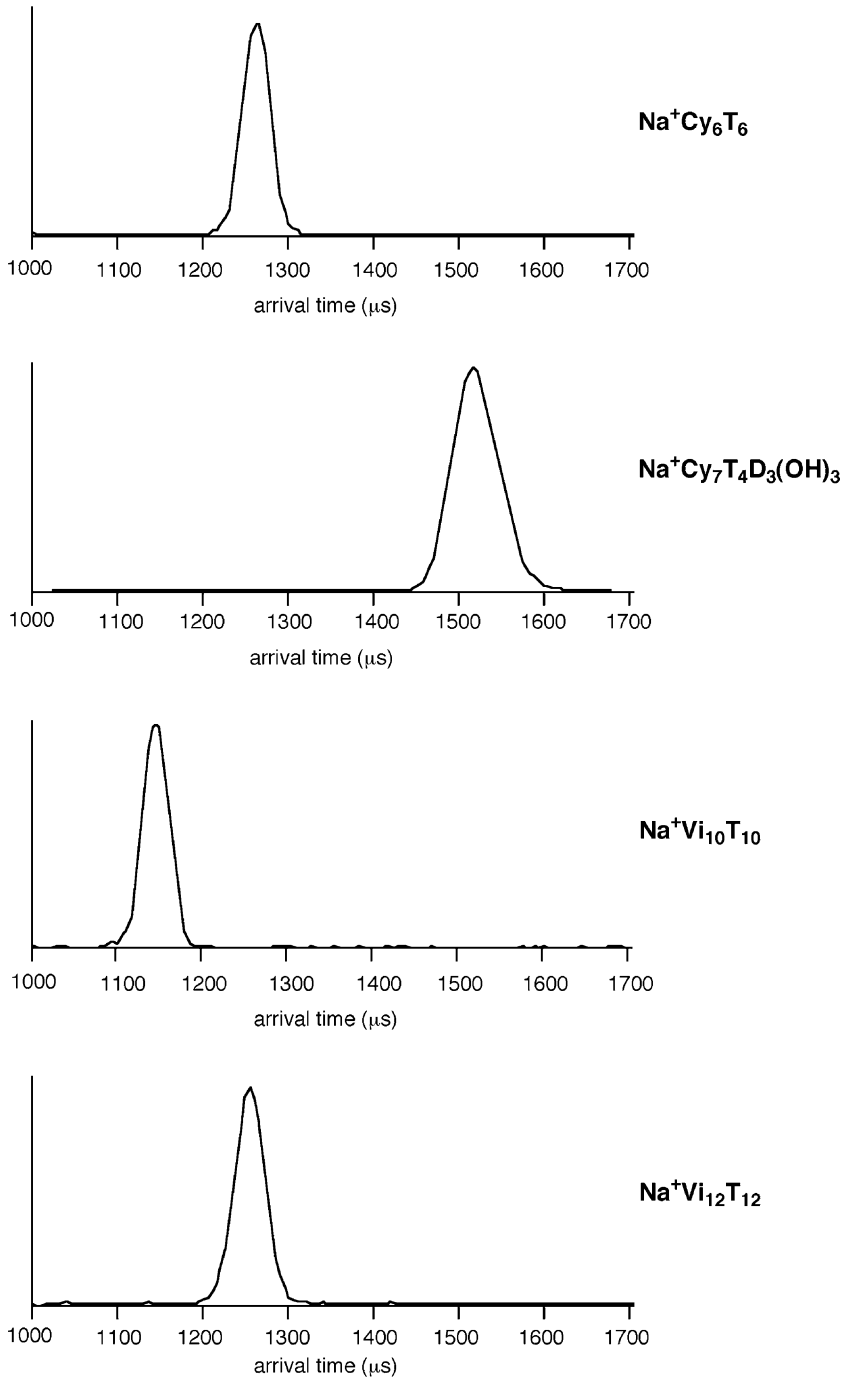

Fig. 5. Typical ATDs for selected Na^+POSS compounds measured on the MALDI-TOF instrument at a temperature of 300 K. Single peaks are observed for all of the POSS compounds on the MALDI-TOF and the ESI instruments. Longer arrival times indicate larger collision cross-sections.

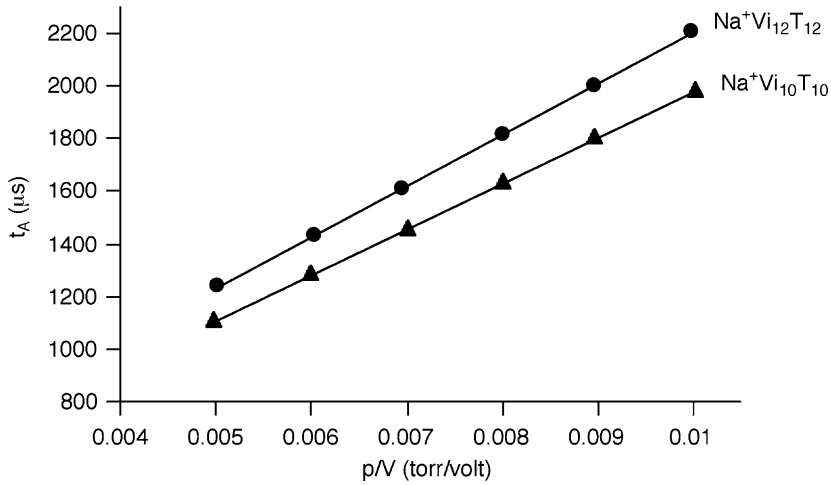

Fig. 6. Plot of experimental arrival time (t_A) vs. p/V (p is the pressure of the He gas in the drift cell and V is the voltage drop across the cell) for $Na^+Vi_{10}T_{10}$ (▲) and $Na^+Vi_{12}T_{12}$ (●). The slope is inversely proportional to the mobility (K_o) and the intercept yields t_o (see Eq. (1)).

quantitative guidelines. The experimental and X-ray cross-sections are very similar to each other for all of the POSS systems, with differences between 1 to 2%. Thus, the POSS compounds do indeed retain their solid-state conformations in the gas phase (or at least to a high degree). The single peaks observed in the ATDs, therefore, are most likely due to single conformations of the Na^+POSS ions and not multiple conformers that are rapidly interconverting.

The cross-sections of the theoretical structures are listed with the experimental and X-ray values in Table 2 as well. Approximately 50–100 low energy structures and their corresponding cross-sections were calculated for each POSS system using the methods described in the Section 2. For each POSS system, the average cross-section of the lowest ∼3 kcal/mol structures (80–90% of the total) is given in the table. MD simulations at 300 K were also performed on the lowest energy structures to determine thermally averaged cross-sections for comparison to experiment, but these calculations yielded similar cross-sections as those given in Table 2. The dynamics simulations show only minor structural variations in the shape and position of the "R" substituents.

The lowest energy structures calculated for $Na^+Cp_4D_4(OH)_4$, $Na^+Cy_6T_6$, and $Na^+Vi_{12}T_{12}$ are shown in Fig. 7. These structures are nearly identical to their corresponding X-ray structures, except for the addition of Na^+. However, the Na^+ ion does not significantly alter any structural aspect of the POSS cage. The metal cation remains outside of the Si–O cage and simply binds to one to two oxygen atoms in the Si–O or to the substituent groups. For example, in $Na^+Cy_6T_6$, the Na^+ ion binds to two oxygen atoms in the Si–O cage. For $Na^+Vi_{12}T_{12}$, the Na^+ ion binds to one oxygen atom in the Si–O cage but also "binds" to two neighboring vinyl groups. For $Na^+Ph_8T_8$, the Na^+ ion does not bind to the Si–O cage at all and is, instead, sandwiched between two neighboring phenyl groups. In the incompletely condensed POSS systems, the Na^+ ion binds to the available OH sites. However, the overall shape of the partial Si–O cage is not significantly altered by the presence of the Na^+ ion.

The calculated cross-sections of these theoretical structures agree very well with X-ray and experimental values, with differences ranging between 1–2%. This is typical of the level of agreement between ion mobility experiments and theoretical models obtained for a number of different biological and synthetic systems that are similar in size as these POSS compounds. This level of agreement also indicates that the new Si parameters used in the calculations are suitable for

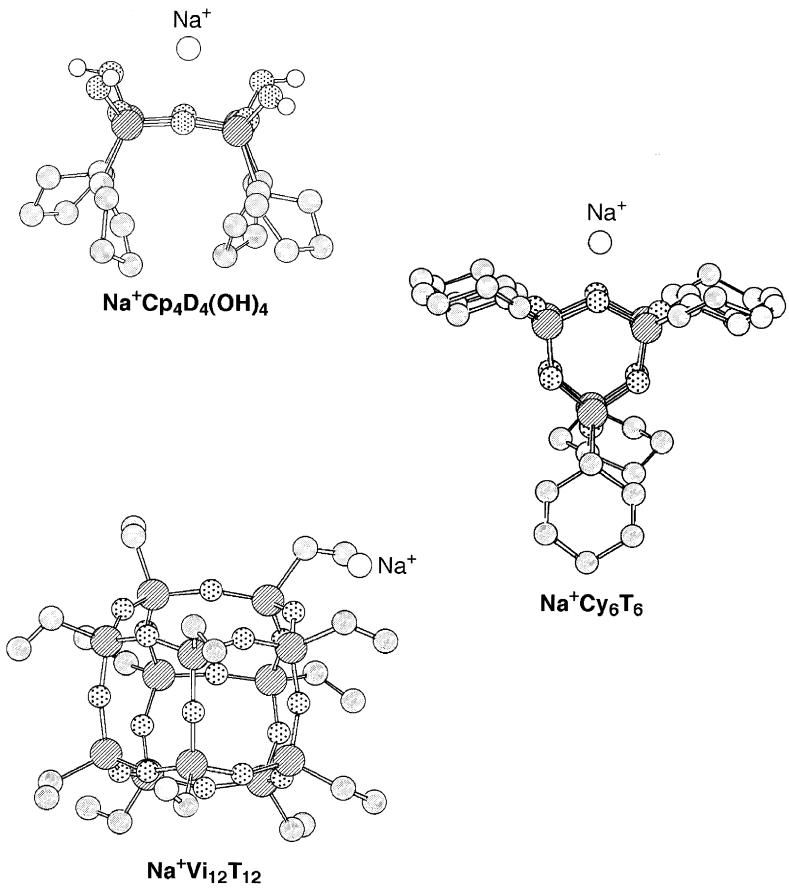

Fig. 7. Lowest energy structures of various Na^+POSS compounds obtained from the AMBER calculations. Silicon atoms are striped, oxygens are spotted, carbons are gray, and hydrogens are white. The Na^+ ion always remains outside of the Si–O cage. The calculated cross-sections of these structures agree very well with experimental and X-ray cross-sections.

modeling these systems, without significant modifications needing to be made to the computational programs. It also generates confidence in using these same calculations, which have already been shown to accurately model gas-phase conformations of synthetic polymers, to model gas-phase conformational properties of POSS–polymer systems that are not well known.

4. Conclusion

Experimental and theoretical parameters have been successfully developed to accurately model the gas-phase conformations of a variety of POSS compounds with different Si–O cage sizes and substituent groups. Collision cross-sections of POSS compounds cationized by Na^+ were measured using ion mobility experiments and MM/MD calculations and compared to calculated values of previously determined X-ray structures. Good agreement between experimental, theoretical, and X-ray cross-sections was observed for all of the POSS systems, with differences falling within 1–2%. Theory indicates that the sodium ion, used to cationize the POSS compounds, essentially acts as a “spectator ion” and simply attaches to oxygens in the Si–O cage or interacts with the substituent groups (vinyl and phenyl). In neither case

does the Na^+ ion significantly alter the structure of the POSS cage. It is hoped that the parameterizations developed in this study can be confidently used to accurately model POSS–polymer systems, in which detailed conformational information is not well known.

Acknowledgements

The support of the Air Force Office of Scientific Research under Grant F49620-99-1-0048 is gratefully acknowledged. We also thank Drs. Tim Haddad and Shawn Phillips for providing samples and X-ray structural parameters.

References

[1] J.D. Lichtenhan, in: J.C. Salamone (Ed.), Polymeric Materials Encyclopedia, CRC Press, New York, 1996, p. 7769.
[2] J.J. Schwab, J.D. Lichtenhan, Appl. Organometal. Chem. 12 (1998) 207.
[3] J.D. Lichtenhan, Y. Otonari, M.J. Carr, Macromolecules 28 (1995) 4355.
[4] F.J. Feher, J.J. Schwab, D.M. Tellers, A. Burstein, Main Group Chem. 2 (1998) 123.
[5] T.S. Haddad, J.D. Lichtenhan, Macromolecules 29 (1996) 7302.
[6] A. Sellinger, R.M. Laine, Macromolecules 29 (1996) 2327.
[7] M.T. Bowers, P.R. Kemper, G. von Helden, P.A.M. van Koppen, Science 260 (1993) 1446.
[8] D.E. Clemmer, M.F. Jarrold, Mass Spectrom. Rev. 32 (1997) 577.
[9] G. von Helden, T. Wyttenbach, M.T. Bowers, Int. J. Mass Spectrom. Ion Processes 146/147 (1995) 349.
[10] T. Wyttenbach, G. von Helden, M.T. Bowers, Int. J. Mass Spectrom. Ion Processes 165/166 (1997) 377.
[11] J. Gidden, T. Wyttenbach, A.T. Jackson, J.H. Scrivens, M.T. Bowers, J. Am. Chem. Soc. 122 (2000) 4692.
[12] J. Gidden, A.T. Jackson, J.H. Scrivens, M.T. Bowers, Int. J. Mass Spectrom. 10 (1999) 883.
[13] J. Gidden, T. Wyttenbach, J.J. Batka, P. Weis, M.T. Bowers, J. Am. Soc. Mass Spectrom. 10 (1999) 883.
[14] J. Gidden, A.T. Jackson, J.H. Scrivens, M.T. Bowers, J. Am. Soc. Mass Spectrom. 13 (2002) 499.
[15] X-ray structures were obtained from Dr. Tim Haddad at ERC Inc., Air Force Research Laboratory.
[16] T. Wyttenbach, P.R. Kemper, M.T. Bowers, Int. J. Mass Spectrom. 212 (2001) 13.
[17] E. Shammel, P.R. Kemper, J. Gidden, D.P. Fee, M.T. Bowers, manuscript in preparation.
[18] J.B. Fenn, N. Mann, C.K. Weng, S.F. Wong, Mass Spectrom. Rev. 9 (1990) 37.
[19] F. Hillenkamp, M. Karas, R.C. Beavis, B.T. Chait, Anal. Chem. 63 (1991) 1193A.
[20] E.A. Mason, E.W. McDaniel, Transport Properties of Ions in Gases, Wiley, New York, 1988.
[21] D.A. Case, D.A. Pearlman, J.W. Caldwell, T.E. Cheatham III, W.S. Ross, C.L. Simmerling, T.A. Darden, K.M. Merz, R.V. Stanton, A.L. Cheng, J.J. Vincent, M. Crowley, V. Tsui, R.J. Radmer, Y. Duan, J. Pitera, I. Massova, G.L. Seibel, U.C. Singh, P.K. Weiner, P.A. Kollman, AMBER 6.0, University of California, San Francisco, CA, 1999.
[22] T. Wyttenbach, G. von Helden, M.T. Bowers, J. Am. Chem. Soc. 118 (1996) 8355.
[23] T. Wyttenbach, J.J. Batka Jr, J. Gidden, M.T. Bowers, Int. J. Mass Spectrom. 193 (1999) 143.
[24] H. Sun, D. Rigby, Spectrochim. Acta A 53 (1997) 1301.
[25] W.D. Cornell, P. Cieplak, C.I. Bayly, P.A. Kollman, J. Am. Chem. Soc. 115 (1993) 9620.
[26] G. von Helden, M.T. Hsu, N. Gotts, M.T. Bowers, J. Phys. Chem. 97 (1993) 8182.
[27] T. Wyttenbach, G. von Helden, J.J. Batka Jr, D. Carlat, M.T. Bowers, J. Am. Soc. Mass Spectrom. 8 (1997) 275.
[28] J. Gidden, J.E. Bushnell, M.T. Bowers, J. Am Chem. Soc. 123 (2001) 5610.